Received: 12 September 2020 | Revised: 9 October 2020 | Accepted: 13 October 2020

DOI: 10.1111/cas.14696

ORIGINAL ARTICLE

Cancer Science WILEY

Prolonged unfolded protein reaction is involved in the induction of chronic myeloid leukemia cell death upon oprozomib treatment

Fang Wang[1] | Xin Wang[2] | Na Li[1] | Juan Liu[3] | Lin Zhang[1] | Lingyun Hui[1] | Ai Feng[1] | Zhonglin Wang[1] | Yawen Wang[1,2]

[1]Department of Laboratory Medicine, The First Affiliated Hospital of Xi'an Jiaotong University, Xi'an, China

[2]Biobank, The First Affiliated Hospital of Xi'an Jiaotong University, Xi'an, China

[3]Department of Hematology, The First Affiliated Hospital of Xi'an Jiaotong University, Xi'an, China

Correspondence
Yawen Wang, Department of Laboratory Medicine/Biobank, The First Affiliated Hospital of Xi'an Jiaotong University, No. 277, Yanta West Rd, Xi'an, Shaanxi Province 710061, China.
Email: wfang1823@xjtu.edu.cn

Funding information
Clinical Research Award of the First Affiliated Hospital (grant/award number: XJTU1AF-CRF-2015-009); Natural Science Foundation of Shaanxi Province (grant/award number: 2019DLSF03-02); National Natural Science Foundation of China (grant/award number: 81600134).

Abstract

To select the most efficient chemical to induce apoptosis in leukemia cells, a multi-drug screen was applied on bone marrow mononuclear cells from chronic myeloid leukemia (CML) patients. Oprozomib (Cpd 21) was chosen for the subsequent experiments. The isobaric tags for relative and absolute quantitation (iTRAQ) was then performed to identify the responsible pathway relative to apoptosis and the results showed that endoplasmic reticulum (ER) chaperones were upregulated. Apoptosis was attributed to a joint effect of calcium leakage andPERK and IRE1α phosphorylation. The PERK branch was responsible for the first wave of cell death that occurred within 24 hours. The later wave of apoptosis was mediated by IRE1α, which transmit apoptotic signals through the ASK-JNK-BIM axis. Release of Ca2+ from ER into cytosol resulted in activation of calpain, which, in turn, cleaved caspase-12. Our data also explained the selective killing effects of oprozomib on CML cells, which relied on proteasome activity. The present study demonstrated that prolonged inhibition of proteasome to trigger unfolded protein response could be an alternative strategy for treating CML in light of tyrosine kinase inhibitors resistance.

KEYWORDS
apoptosis, CML, ER stress, proteasome inhibitor, unfolded protein reaction

1 | INTRODUCTION

BCR/ABLp210, the molecular marker of chronic myeloid leukemia (CML), with constitutively activated tyrosine kinase activity, drives the development of CML by activating multiple downstream signaling pathways, including RAF/MEK/ERK, PI3K/AKT, and JAK/STAT5.[1] Imatinib mesylate (IM) dramatically improves patients' outcome when used to treat disease in the chronic phase; unfortunately, it is not curative. Resistance to IM, especially in advanced-stage disease, has been recognized as a major challenge. IM resistance is mechanically heterogeneous and may be associated with increased expression of BCR-ABL, ABL kinase domain mutations, quiescent stem cells, or other cytogenetic aberrations.[2,3] Thus, identifying the most effective alternative approaches for patients who fail to achieve a significant therapeutic response is critical.

Fang and Xin equally contributed to this work.

In last dacede, a series of anticancer therapies have been connected with the blockage of the ubiquitin-proteasome system (UPS).[4-6] The UPS accounts for the major component of the cellular protein degradation machinery, with a function to prevent the accumulation of mis/unfolded protein. Deleterious protein targets are polyubiquitylated by three enzymes in a highly coordinated manner through different steps. The ubiquitin is initially activated by ubiquitin-activating enzyme E1 to generate a high-energy thiol ester intermediate; E1-S-ubiquitin is then transferred by the ubiquitin-conjugating enzymes E2 to the substrate that is specifically bound to ubiquitin-protein ligase E3, which catalyzes the covalent attachment of ubiquitin to the substrates. After several rounds of ubiquitylation, the labeled substrate with a polyubiquitin chain is recognized by 19S regulatory particles (19S PR) of the proteasome. The second function of the 19S PR is to facilitate entry of substrate into the proteolytic chamber of 20S core particles (20S CP) of the proteasome. The proteolytic chamber, in which the substrate is degraded into short peptides, is a barrel-shaped structure arranged in four stacked seven-membered rings. Two outer α rings and two inner β rings form the general structure of 20S CP, α1-7β1-7 β1-7α1-7. The peptide hydrolyzing activity of the 20S core is restricted to three β-subunits, β1, β2, and β5, with post-glutamyl peptide hydrolyzing, trypsin-like, and chymotrypsin-like activities, respectively. In some cases, alternative forms of the proteasome, such as the immunoproteasome, in which the three hydrolyzing sites are replaced by the so-called immunosubunits β1i/LMP2, β2i/MECL-1, and β5i/LMP7, are induced and involved in routine proteolytic functions.[7,8]

Proteins synthesized in cancer cells promote cell survival and proliferation, and/or inhibit apoptosis. Appropriate protein degradation by proteasome is fundamental to the activation or inhibition of many cellular processes, such as the cell cycle or apoptosis.[9] Cancer cells with faster protein turnover rate are even more sensitive to the repression of proteasome activity; this notion singles out the proteasome as a unique target for anticancer therapy.[10] In the present study, we demonstrated the pro–apoptotic effects of the immunosubunit β5i/LMP7 inhibitor, oprozomib, on CML cells derived from clinical patients and further studied the underlying molecular basis by which the oprozomib triggered cell death. Our data indicated that loss of proteasome activity sensitizes CML cells to apoptosis, providing a promising alternative strategy for overcoming IM resistance.

2 | MATERIALS AND METHODS

2.1 | Main reagents

Antibodies used for detection of UPS and unfolded protein response (UPR) signals as well as caspase-3 and 12 and poly ADP ribose polymerase (PARP) were purchased from Cell Signaling Technology. Antibodies for Bim, p-Bim, Bid, Puma, Noxa, and GAPDH were purchased from Santa Cruz Biotechnology. Antibodies for ITPR2 were purchased from Abcam, and a Co-Immunoprecipitation Kit was purchased from Pierce. The custom inhibitor library (Table S1) was purchased from Selleck Chemicals. Salubrinal, selonsertib, PTFα, STF081030, and Kira6 were purchased from Sigma-Aldrich. A Calpain Activity Assay Kit was purchased from Abcam.

2.2 | Primary chronic myeloid leukemia cells

Stated in document S1. Supporting materials and methods.

2.3 | Proteasome activity and calpain activity

Proteasome and calpain activity were performed using a proteasome activity assay kit (ab107921, Abcam) and a calpain activity kit (ab65308, Abcam) according to manufacturer's protocols.

2.4 | Statistical analysis

The data were expressed as $X \pm SD$ (n = 3). The difference between each group was evaluated using Student's *t*-test. $P < 0.05$ was considered statistically significant.

Methods for the rest of the assays, including Cell Counting Kit-8 (CCK-8), intracellular Ca^{2+} detection, western blotting, co–immunoprecipitation, iTRAQ and parallel reaction monitoring (PRM), are stated in document S1.

3 | RESULTS

3.1 | Oprozomib (Cpd 21) showed the most potent effect on induction of apoptosis

Forty-three inhibitors (Table S1) were used for drug screening in mononuclear cells of bone marrow derived from patients with CML. Four inhibitors (Compound 6, quisinostat, Cpd 13, givinostat, Cpd 21, oprozomib, Cpd 40, BIX 01294) were found to dramatically suppress the viability of cells from all five patients (Figure 1, A), among which two patients in blast crisis showed weak response to imatinib administration (Table S2, Figure S1). We also found that Cpd 21 suppressed colony forming ability in progenitor cells (unpublished data), indicating that the potential of Cpd 21 was not limited to mature cells that accounted for the majority of bone marrow mononuclear cells (BM-MNC). A more than 50% decrease in viability was observed in all tested cells with treatment of four individual inhibitors. The IC50 values of each inhibitor were then determined using cells from another three patients. Cpd 21, with the lowest IC50, ranging from 0.15 to 0.35 μM in three tested cells, was identified as the best potential candidate (Figure 1, B). Cpd 21 was the most effective candidate to provoke apoptosis (>50% in all tested cells) (Figure 1, C). In cells from bone marrow of three healthy donors, there was no significant difference in cell death between groups with or without Cpd 21 treatment (Figure 1, D). These data suggested that Cpd 21

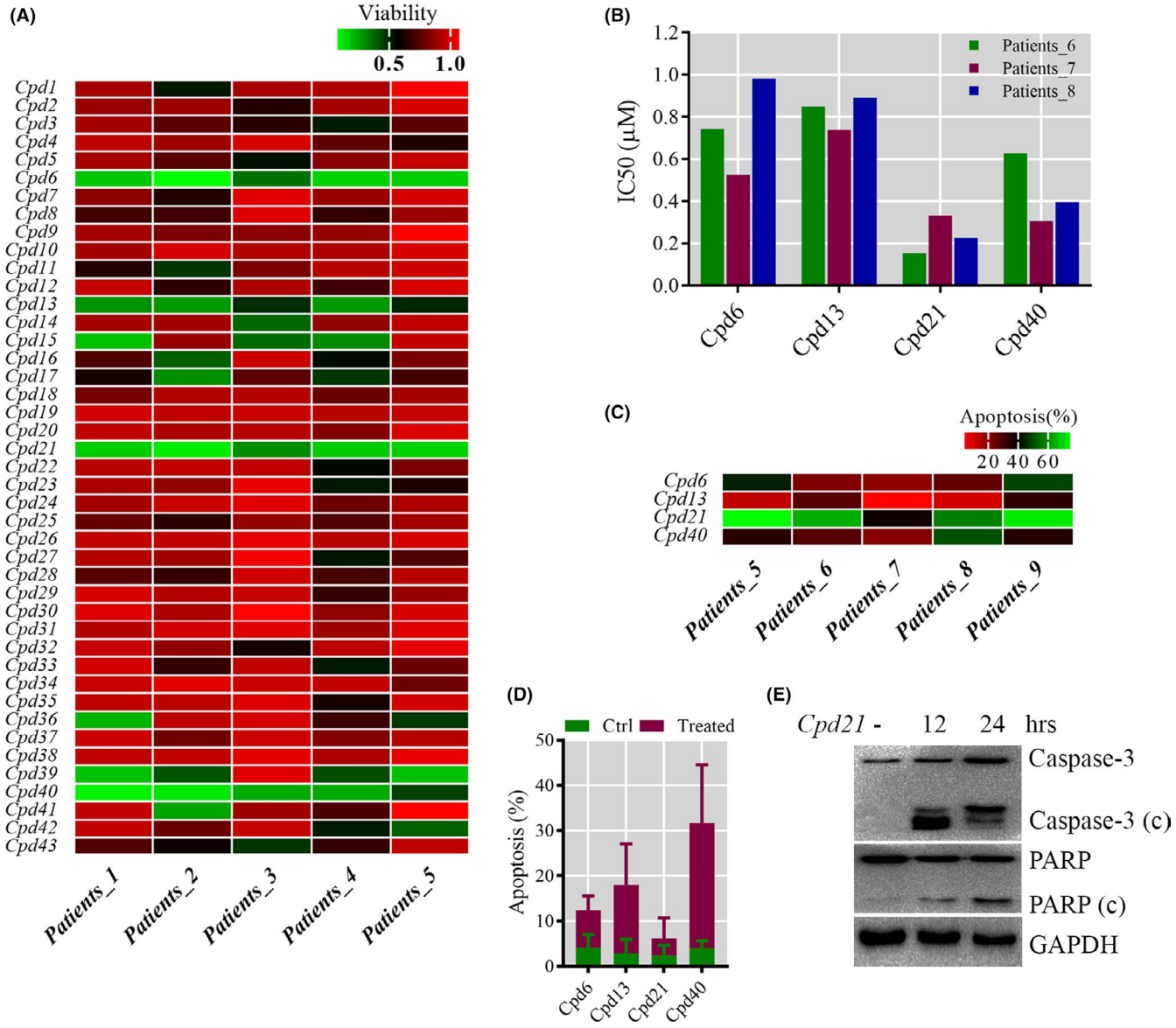

FIGURE 1 Drug screening identified oprozomib as the most potent agent to induce apoptosis in chronic myeloid leukemia (CML) bone marrow cells. A, Viability of bone marrow mononuclear cells derived from five CML patients was determined in the presence of 43 compounds. Cells were treated with indicated compound at 1 μM for 48 h. Viability was tested by Cell Counting Kit-8 (CCK-8). B, IC50 of four compounds for 48 h was determined by CCK-8. C, Apoptosis induced by four compounds after 48 h treatment at average IC50 was measured by flow cytometry (FCM). D, Cytotoxicity of four compounds on bone marrow mononuclear cells (BM-MNC) from healthy donors. Cells treated with indicated compounds, each compound was used at average IC50 that calculated from 3 patient-derived cells (fig 2B). E, Oprozomib (Cpd 21) triggered processing of caspase-3 and downstream substrate poly ADP ribose polymerase (PARP)

is a promising compound to specifically kill CML cells, which barely even responded to IM. We also verified the cleavage fragments of caspase-3 and its substrate PARP, which became detectable after Cpd 21 treatment for both 12 and 24 hours (Figure 1, E).

3.2 | Cpd 21 triggered unfolded protein response following accumulation of ubiquitinated proteins

Cpd 21 was developed as a next-generation orally bioavailable irreversible inhibitor for CT-L activity of 20S proteasome β5/LMP7. Cpd 21 significantly inhibited the CT-L activity (Figure 2, A) but had little effect on the abundance of LMP7 (Figure S2). It has been well documented that the proteasome is the crucial component for the degradation of unwanted proteins.[9] Therefore, inhibition of the proteasome may suspend degradation of detrimentally undesired proteins which were tagged with ubiquitin by the ubiquitin-proteasome system. The ubiquitinated proteins were then determined in BM-MNC from four patients, and the data confirmed the increase in ubiquitinated proteins (Figure 2, B). Next, the iTRAQ was applied to further elucidate the molecular connection between proteasome inhibition and apoptosis. The BM-MNC from six patients

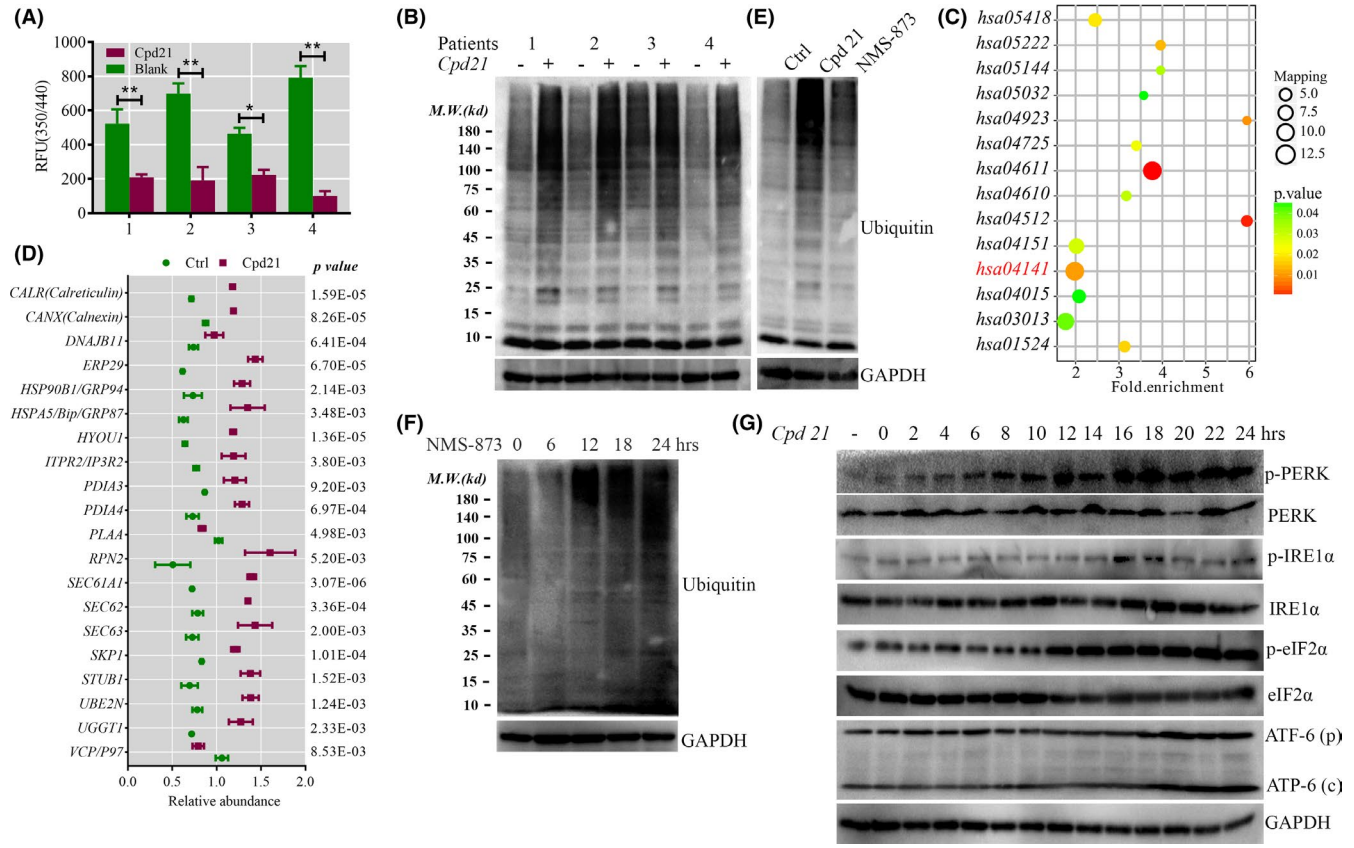

FIGURE 2 Oprozomib exposure inhibited proteasome activity and launched unfolded protein response (UPR). A, CT-L activity of proteasome was suppressed by oprozomib. B, Oprozomib increased ubiquitin-tagged proteins after blockage of proteasome activity. C, Pathway enrichment of the upregulated proteins. has 04141 (marked by red color) was selected for further investigation. D, Parallel reaction monitoring validation of differentially expressed proteins that enriched in pathway has 04141. E,F, NMS-873 treatment resulted in rise of ubiquitin-tagged proteins in a time-dependent fashion. G, Oprozomib triggered UPR activation. Data from three parallel tests are presented as mean ± SD. $^{*}P < 0.05$, $^{**}P < 0.01$

were treated with Cpd 21 for 36 hours and the lysates were pooled with equal proportion to minimize the difference between individual samples. We finally identified 194 upregulated and 224 downregulated proteins in the presence of Cpd 21 as the fold change was set as 1.5 (Table S3). The upregulated proteins were mainly involved in 14 pathways (Figure 2, C), among which hsa04141 (protein processing in endoplasmic reticulum [ER], red color) (Figure S3) received the most attention. The differentially expressed proteins that belong to hsa04141 were then validated by PRM (Figure 2, D). The Bip (HSPA5/GRP87), a key chaperone in ER lumen that functions as a sensor of undesired proteins, was upregulated more than twofold. Induction of other chaperones such as HSP90B1, UGGT1, and HYOU1 occurred, as well was an adaptive reaction in response to accumulation of the ubiquitinated proteins. It is worth noting that the amount of VCP/P97 and PLAA was unexpectedly decreased (Figure 2, D). VCP/P97 facilitates retro-translocation of un/misfolded proteins in the ER, an indispensable process during ER-related degradation of un/misfolded proteins.[11] Suppression of VCP/P97 blocked ER-associated protein degradation (ERAD), resulting in the rise of ubiquitinated proteins, which was then confirmed by the administration of NMS-873, a selective allosteric VCP/p97 inhibitor, improving the production of ubiquitinated proteins in a time-dependent manner (Figure 2, E,F). Disruption of removal of undesired proteins is closely related to the initiation of UPR; therefore, we examined the activating status of three UPR markers, PERK, IRE1α, and ATF6. Elevated phosphorylation levels of PERK and IRE1α and enhanced ATF6 cleavage were found at 4, 12, and 20 hours, respectively (Figure 2, G), indicating the launch of URP.

3.3 | PERK-eIREα-ATF4 mediated the first wave of apoptosis

The PERK was the first activated UPR marker. As dissociation with Bip is the prerequisite of PERK auto–phosphorylation,[12,13] we first verified the decrease in Bip-bound PERK, which became remarkable within 6 hours, while the interaction between Bip and ubiquitinated proteins was correspondingly improved time-dependently (Figure 3, A). As an adaptive response, UPR was programmed to restore the homeostasis by mitigating protein misfolding.[14,15] A short time pause in protein synthesis is beneficial through reducing the overall peptide load in ER lumen, while the prolonged block in translation due to sustained PERK pathway activation is more likely incompatible with cell survival.[16,17] In this regard, Cpd 21 was withdrawn at different

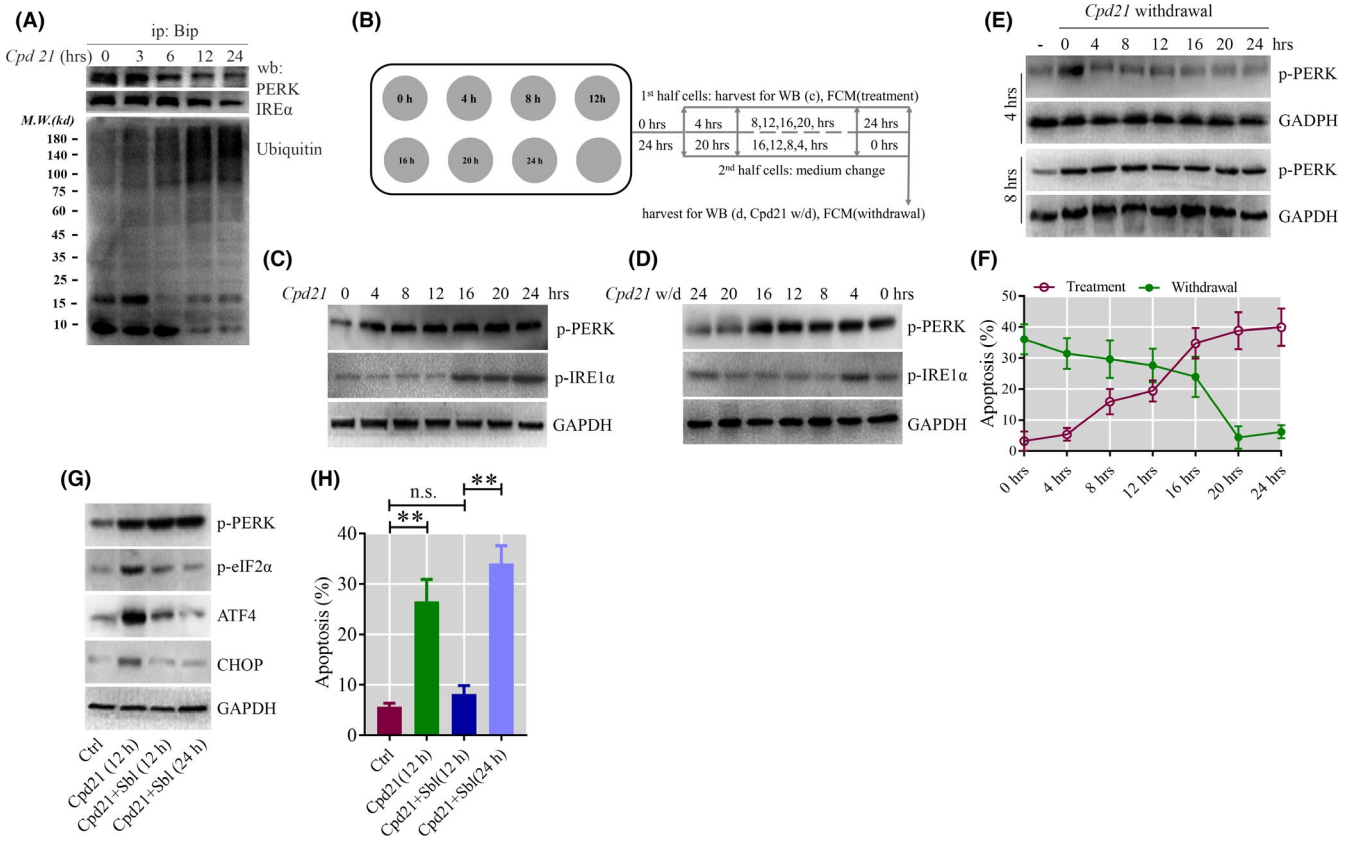

FIGURE 3 PERK branch of unfolded protein response (UPR) was responsible for the first wave cell death. A, Disassociation of PERK and IREα with Bip started within 6 h in the presence of oprozomib. B, Flowchart for investigating the role shift of UPR from cytoprotection to cytotoxicity. C, Phosphorylation of PERK and IREα at different time points. D, Phosphorylation of PERK became irreversible if the oprozomib treating time lasted for more than 4 h. Lane 2, w/d 20 stands for after oprozomib withdrawal; the cells were cultured in drug-free medium for another 20 h. E, PERK dephosphorylation after 4-h (upper) or 8-h (lower) treatment. The indicated time at the top represents the duration of drug-free culture after oprozomib withdrawal. F, Apoptosis induction at indicating treating time (aubergine) or time of drug-free culture according to the description in (B). G, eIF2α phosphorylation and ATF4, CHOP upregulation induced by oprozomib; the effect was blocked by co–treatment with salubrinal (Sbl) (300 nM). H, Salubrinal inhibited apoptosis at 12 h but failed at 24 h. For western blot, cells from patients were separated and treated as stated in Figure 1C; the lysates were collected and stored at −80° and the test was conducted using a pool of lysates from several patients, presented in Table S2. For apoptosis assay, Flow cytometry (FCM) test was conducted for individual patients after treatment if the cells were sufficient. Data from three parallel tests are presented as mean ± SD. $^{**}P < 0.01$

time points to study how the signaling shifted from the cytoprotective role to the induction of apoptosis (Figure 3, B). For the first half of the cells in each group, which were harvested at indicated time points, treatment for 4 hours was sufficient to increase the PERK phosphorylation (Figure 3, C, lane2), which, however, appeared to be reversed by drug withdrawal (Figure 3, D, lane2) in the second half of the cells, which were cultured in drug-free medium for the indicated time after Cpd 21 withdrawal and finally collected together. It is noteworthy that the phosphorylation of PERK became irreversible if the treatment time was doubled (8 hours) or longer (Figure 3, C, lane3,4 vs Figure 3, D, lane3,4). To rule out the possibility that the maintenance of PERK phosphorylation in 8-hour-treated cells resulted from culturing in the drug-free medium for a relatively shorter time, cells treated with Cpd 21 for 4 or 8 hours were transferred to drug-free conditions and collected respectively at different time points. The results clearly showed that for cells treated for 4 hours, dephosphorylation of PERK occurred within 4 hours after Cpd 21 withdrawal (Figure 3, E, upper). However, for those with 8-hour treatment, PERK phosphorylation was sustained all through the culturing without Cpd 21 (Figure 3, E, lower). In the Figure 3B scenario, compared with 4 hours of treatment for which no significant apoptosis was detected (Figure 3, F, aubergine line, 4 hours), 8-hour treatment brought about marked cell death (Figure 3, F, aubergine line, 8 hours) and further improvement, although the drug has been withdrawn (Figure 3, F, green line, 16 hours). We next investigated the status of downstream signals. Phosphorylation of eIF2α, induction of ATF4, and CHOP were confirmed (Figure 3, G). To further verify that the eIF2α-ATF4-CHOP chain was involved in p-PERK-induced apoptosis, salubrinal, an eIF2α inhibitor, was used to block signal transduction to AFT4. As expected, salubrinal hampered eIF2α phosphorylation and prevented upregulation of ATF4 and CHOP (Figure 3, G), leading to striking reduction in apoptosis at 12 hours (Figure 3, H). Intriguingly, we also found evident apoptosis if the time was extended to 24 hours (Figure 3, H) as the eIF2α was still blocked (Figure 3, G). These results demonstrated the contribution of the PERK branch to Cpd 21-triggered apoptosis, which,

probably depended not only on PERK. In view of the inhibiting effects of salubrinal on apoptosis at 12 hours, we speculated that the PERK may merely represent the first wave of cell death followed by the involvement of other pathways.

3.4 | IRE1α mediated cell death through upregulation of Bim

IRE1α activation by auto–phosphorylation relies on dissociation with Bip (Figure 3, A). Elevated IRE1α phosphorylation became prominent at 16 hours (Figure 3, C). We therefore supposed that IRE1α was responsible for the later onset of cell death. Activated IRE1α acted as a scaffold, allowing its interaction with ASK and TRAF2,[18] forming the IRE1α-TRAF2-ASK1 complex, which was then confirmed by an increase levels of IRE1α-engaged ASK and TRAF2 in the presence of Cpd 21 for 16 hours (Figure 4, A). We observed that the interaction of adapter TRAF2 with IRE1α evoked a cascade of phosphorylation events that ultimately activated c-JNK (Figure 4, B). c-JNK is documented to be activated to impact the apoptosis machinery via regulation of the balance of pro/anti–apoptosis members of Bcl-2 family.[19] Among the four members that were tested, Bim was distinctly upregulated (Figure 4, C). Bim phosphorylation, which was reported to bind and neutralize Bcl-2, was clearly reinforced (Figure 4, D). To determine whether the induction and modification of Bim were linked to the IRE1α-TRAF2-ASK1-c-JNK cascade, selonsertib, an ASK1 inhibitor, was used to attenuate the phosphorylation of ASK1. The results showed a decline in Bim expression (Figure 4, C) and phosphorylation (Figure 4, D) under the combination of selonsertib and Cpd 21. As a result, co–treatment with selonsertib led to apoptosis retardation, which was further strengthened by salubrinal (Figure 4, E). Neither alone nor in company with salubrinal did selonsertib fully inhibit the Cpd 21-induced apoptosis, indicating that other than PERK and IRE1α, more pathways were implicated. Meanwhile, our data suggested that reinforced Bim activity was independent of P53, as neither abundance nor phosphorylation level was influenced by PTFα addition (Figure 4, F). To further exclude the implication of P53 in Bim regulation, we treated K562, a P53 deficient cell line, with Cpd 21 for the indicated time or at indicated concentrations. Levels of total and phosphorylated Bim were both increased in a time and dose-dependent fashion (Figure 4, G). We further examined whether IRE1α, the dominant activator of ASK-1 in the context of Cpd 21,

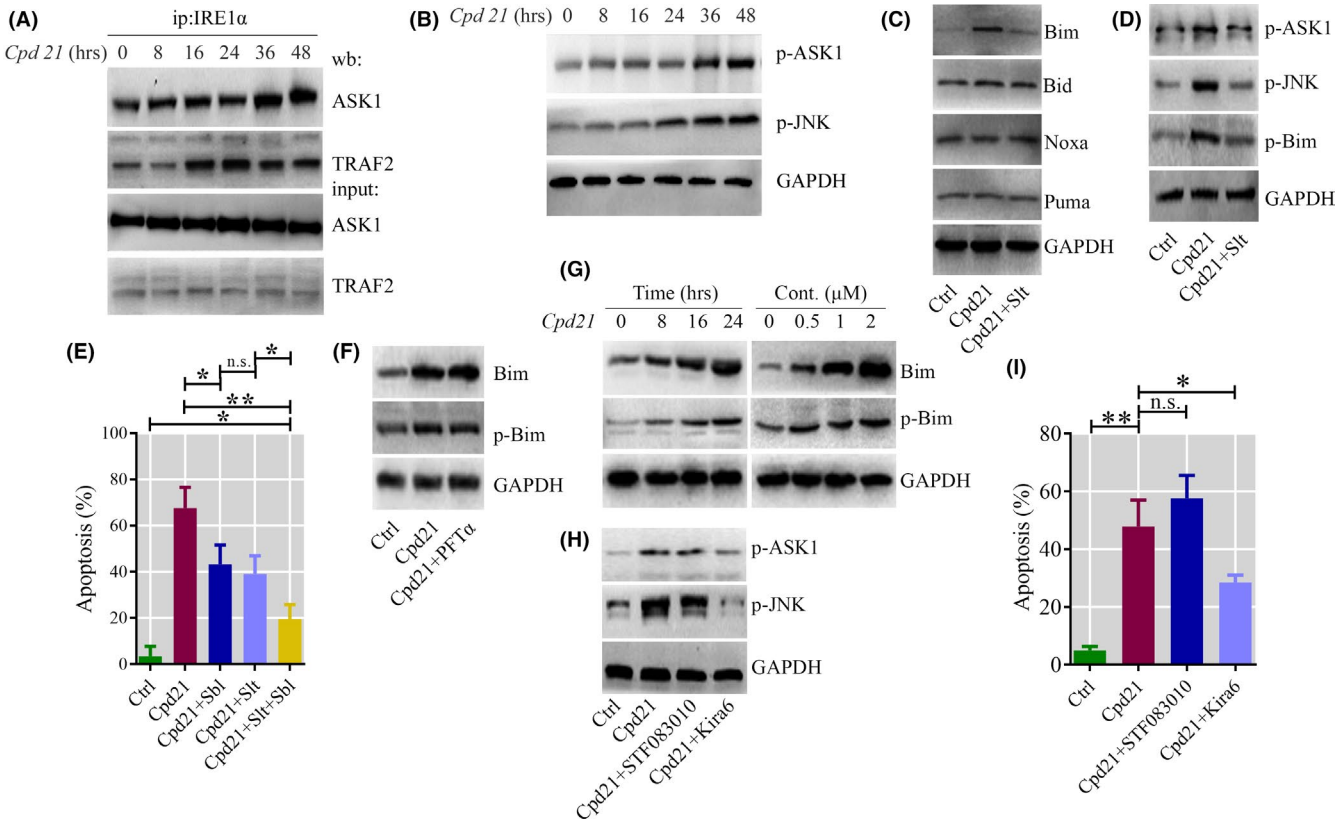

FIGURE 4 Activation of IREα branch. A, Association of IREα with ASK1 and TRAF2 was improved at 36 and 16 h, respectively, post–oprozomib administration. B, Phosphorylation of ASK1 and TRAF2. Upregulation (C) and phosphorylation (D) of Bim were measured at 48 h post–oprozomib administration, which was blocked by selonsertib (Slt) (500 nM), an ASK1 inhibitor. E, Combination of selonsertib and salubrinal further inhibited oprozomib-induced apoptosis in comparison with selonsertib or salubrinal alone (48 h). F, Upregulation and phosphorylation of Bim were not affected by P53 blockage (48 h). G, Upregulation and phosphorylation of Bim tested in K562 cells in a time and dose-dependent fashion. H, Activation of ASK1 and JNK at 48 h was independent of endonuclease activity of IREα. I, Kira6 but not STF083010 significantly reduced apoptosis induction by oprozomib (48 h). Data from three parallel tests are presented as mean ± SD. $^{**}P < 0.01$

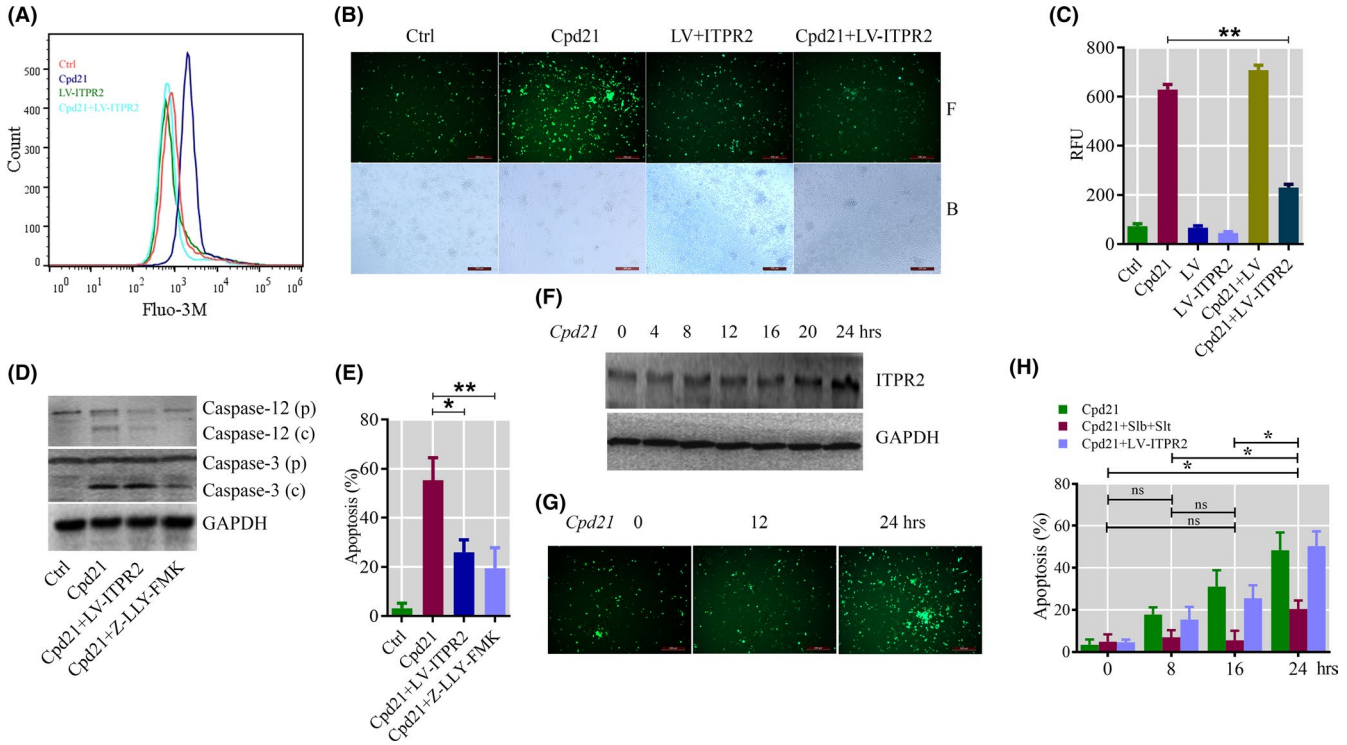

FIGURE 5 ITPR2-mediated Ca2+ efflux. Cytosolic Ca2+ was detected by Fluo-3 staining using flow cytometry (A) and a fluorescent microscope (B) at 48 h post–oprozomib treatment. Lentivirus vector containing siRNA-targeted ITPR2 (LV-ITPR2) was applied to downregulate the ITPR2 and subsequently inhibited Ca2+ release. C, LV-ITPR2 suppressed the calpain activity that increased as a result of Ca2+ accumulation in cytosol. D, Caspase-12 was the downstream target of Ca2+ Calpain signal. E, LV-ITPR2 block in part apoptosis. F, ITPR2 expression induction in the presence of oprozomib was time-dependent and became obvious at 24 h post–oprozomib exposure. As a consequence, cytosolic Ca2+ increased remarkably at this time (G). H, Induction of apoptosis mediated by ITPR2 occurred at 24 h post–oprozomib addition. Data from three parallel tests are presented as mean ± SD. $^{*}P < 0.05$, $^{**}P < 0.01$

induced UPR. STF081030 and Kira6, two mechanically distinct inhibitors of IRE1α, were then employed. STF083010, which attenuates endonuclease activity without affecting its kinase activity, did not diminish the phosphorylation of ASK1 and downstream c-JNK. While Kira6, which inhibits both endonuclease and kinase activity, clearly lessened the quantity of phosphorylated ASK1 and c-JNK, supporting that Cpd 21-provoked ASK1 activation relied mainly on the kinase activity (Figure 4, H). We finally examined the contribution of endonuclease of IRE1α to the induction of apoptosis. Instead of reducing them, SFT083010 administration even slightly promoted cell death, suggesting that the endonuclease activity of IRE1α was more likely cytoprotective[20]. We speculated that blockage of this activity may switch the signals towards pro–apoptosis, which was covered by the activation of ASK1. In addition, Kira6 significantly reduced the apoptosis, suggesting the pro–apoptotic function of kinase activity of IRE1α (Figure 4, I).

3.5 | Caspase-12 processing in Cpd 21-treated cells through calpain activated by calcium efflux

Our differentially expressed data showed increased ITPR2 abundance (Figure 2, D). We questioned the possibility that apoptosis may have resulted partly from disruption in Ca2+ homoeostasis because ITPR2 is a major regulator of Ca2+ concentration in ER lumen.[21] Cpd 21 promoted cytoplasmic Ca2+ accumulation, which was then abolished by ITPR2 depletion (Figure 5, A,B). It is well established that the cytoplasmic protease calpain played roles in apoptosis by cleaving diverse targets and thereby may be actively involved in cell death. Caspase-12 is a well-defined target of calpain.[22,23] Calpain was activated in a Ca2+-dependent manner and, in turn, cleaved and activated caspase-12, which, bypassing the release of cytochrome C and activation of caspase-9, directly activated the effecter caspase-3. Hence, we next determined the activity of calpain. An approximate 7-fold increase in calpain activity was detected, which largely diminished as ITPR2 siRNA was employed (Figure 5, C). Upon Cpd 21 treatment, we observed the cleaved fragment, which receded when ITPR2 was silenced or calpain was inhibited. However, the downstream caspase-3 processing continued despite full blockage of caspase-12 (Figure 5, D). We supposed that the activation of caspase-3 was a cumulative consequence of IRE1α phosphorylation and Ca2+ efflux. Subsequently, we observed that the ITPR2-deficient cells were resistant to Cpd 21-induced apoptosis, which was also weakened by calpain inhibition (Figure 5, E). We further investigated whether the ITPR2-Ca2+-Calpain-induced apoptosis was in a time-dependent manner and the precise time point did this branch participate in cell death. ITPR2 upregulation was detected at 20 hours after Cpd 21 addition (Figure 5, F), indicating that the

increase in ITPR2 level was a later event in comparison with PERK. Furthermore, Ca2+ release was observed at 24 hours (Figure 5, G), which was consistent with ITPR2 upregulation. We supposed that the total apoptotic effects were attributed to the three components: PERK, IRE1α, and ITPR2. To highlight the contribution of ITPR2, we blocked PERK and IRE1α arms with the combination of SIb and SIt (C+S+S, CSS group). The flow cytometry results clearly showed that apoptosis in the CSS group was remarkably increased at 24 hours (Figure 5, H). In conclusion, our data supported a two-staged apoptosis model induced by the proteasome inhibitor oprozomib within 24 hours of treatment.

3.6 | Ubiquitin-proteasome system proteins and proteasome activity in chronic myeloid leukemia cells

We examined the underlying reason that oprozomib selectively induced CML cell death. We first tested the CT-L activity of proteasome in BM-MNC from heathy donors and CML patients. The results clearly showed enhanced proteasome activity in CML patient-derived bone marrow (BM) cells (Figure 6, A). We also measured the proteasome activity in peripheral blood mononuclear cells (PB-MNC) from these two groups, and similar results were seen (Figure 6, B). We next compared the proteasome activity between bone marrow and peripheral blood from the same individuals, including a total 10 CML patients. No difference was found within each patient (Figure 6, C). Finally, we analyzed the abundance of three UPR molecules. In CML cells, Bip was distinctly upregulated as compared with healthy donors, although only three samples were available for the test. However, both p-PERK and p-IRE1α were not found to be expressed differentially (Figure 6, D). These data indicated that more robust proteasome activity was required for leukemia cells to deal with the un/misfolded proteins that produced along with the relatively rapid protein turnover, a property of tumor cells to fulfill their uncontrolled growth. Elevation of Bip but not p-PERK and p-IRE1α reflected the cytoprotective role of UPR. The stress caused by un/misfolded proteins was compromised by the boosted chaperoning ability of tumor cells before reaching the extent of transcriptional inhibition.

4 | DISCUSSION

Our data provide evidence that the proteasome inhibitor oprozomib induces ER stress and UPR, and eventually transmits the signaling towards cell death in primary CML cells. The pro–apoptotic effects of oprozomib on CML cells derived from clinic patients at different stages with various sensitivity to imatinib treatment, implying that potency of oprozomib was not influenced by the phases of disease. Compared to tyrosine kinase inhibitors (TKI) that specifically target and disable Bcr/Abl fusion protein, oprozomib-evoked reduction of proteasome activity may represent a more general anti–tumor strategy. Cells from AP or BC usually harbor additional chromosome abnormalities,[24] rendering them more likely independent on the signals downstream of Bcr/Abl. Additional mutations offer cells a compensatory mechanism to sustain their survival when the Bcr/Abl

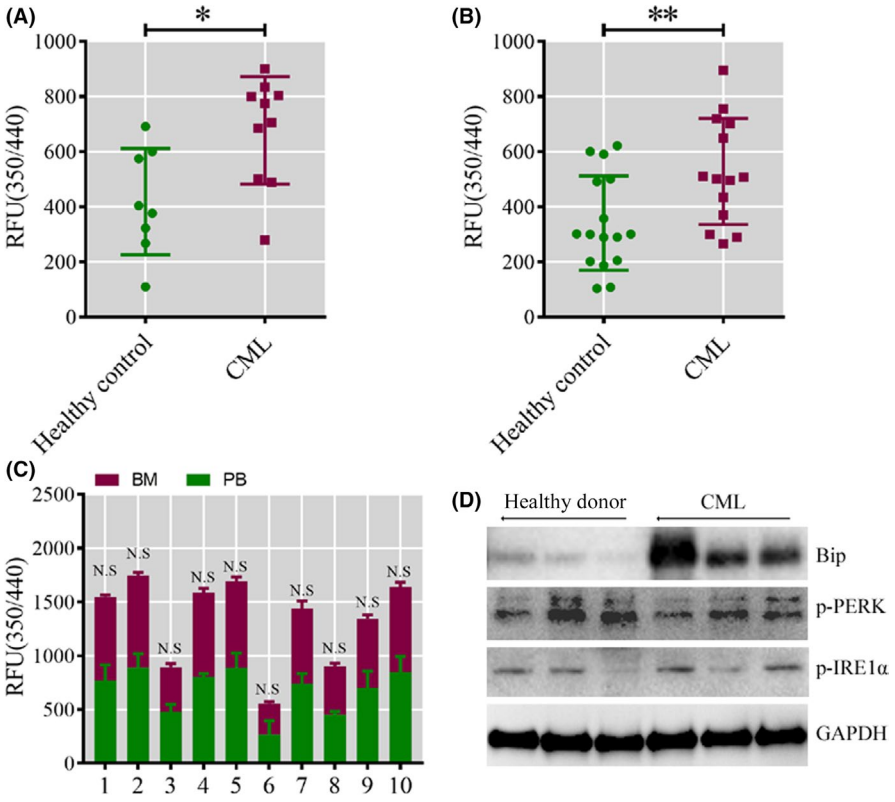

FIGURE 6 Comparison of proteasome activity between heathy donors and chronic myeloid leukemia (CML) patients. CT-L activity of proteasome in bone marrow mononuclear cells (BM-MNC) (A) and peripheral blood mononuclear cells (PB-MNC) (B) from CML patients was significantly higher than for heathy counterparts. C, No difference in CT-L activity of proteasome was observed between BM-MNC and PB-MNC from 10 CML patients. D, Comparison of Bip, p-PERK, and p-IRE1α levels in three chronic myeloid leukemia (CML) patients with three heathy donors. Data from three parallel tests are presented as mean ± SD. $^{*}P < 0.05$, $^{**}P < 0.01$, n.s., not significant

is inactivated. Due to rapid protein turnover, however, they cannot tolerate the defect of proteasome activity, which is responsible for protein homeostasis that is critical to cancer cell survival.[10] Previous studies[25,26] have confirmed the enhanced proteasomal activity in cancer cells and this alteration is crucial to the maintenance of the transformed phenotype. Newly synthesized proteins in proliferating cancer cells are mechanistically connected with increased proteasomal activity, because cells require a more robust proteasome system to alleviate the cytotoxicity of misfolded proteins produced during the cell cycle.[27] This may explain why malignant cells are more susceptible to proteasome inhibitor-induced cell death.

Proteasome inhibitors provoked ER stress and consequent UPR, which primarily serves as a cytoprotective response to accumulation of harmful misfolded proteins but shifts the signals towards apoptosis with prolonged stress.[28,29] Our iTRAQ data indicated that 18 and 2 proteins enriched in protein processing in the ER pathway (has04141) were upregulated and downregulated respectively. VCP/P97 and PLAA/DOA1 played roles in ERAD, in which the un/misfolded proteins are exported into the cytoplasm and degraded by proteasome. VCP was considered necessary for extraction of proteins from the ER lumen into cytosol, a process named retro-translocation. siRNA-mediated loss of VCP itself resulted in the onset of UPR.[30] The mechanism by which oprozomib decreased VCP level remains elusive. We suppose that the enervation of the retro-translocation resulting from VCP level decrease may be the molecular bridge between proteasome inhibition and initiation of UPR.[31] Among the 18 upregulated ER-resident chaperones, Bip/GRP87 was the central regulator.[12] Increasing evidence revealed that Bip/GRP87 plays critical roles in cytoprotection and cancer development.[32] Bip/GRP87 overexpression was demonstrated in multiple types of solid tumors.[33-35] The induction of Bip/GRP87 is attributed to cells' adaption to the tumor microenvironment.[36] Our data showed that with oprozomib, the elevation of ubiquitinated proteins that associated with Bip/GRP87 reflected this cytoprotective effect of Bip/GRP87. In addition to this chaperoning feature, Bip/GRP87 releases PERK and IREα.[12] Our results revealed that PERK was phosphorylated at 4 hours, whereas the IREα phosphorylation lagged behind for 8 hours after oprozomib administration, suggesting a two-wave model of cell death. It is worth noting that remarkable apoptosis was found at 8 hours despite PERK phosphorylation 4 hours earlier. More importantly, 4-hour treatment followed by drug withdrawal failed to evoke apoptosis, indicating that the PERK's function during this period maybe cytoprotective and the duration of stimuli was critical for the signal switch from stress buffering to apoptosis induction.

The later onset of oprozomib-triggered cell death was attributed to the IRE1α branch of UPR. IRE1α underwent phosphorylation at 16 hours, followed by association with TRAF and ASK1, leading to phosphorylation of ASK-1 and its substrate JNK. Among the four Bcl-2 pro–apoptotic members that we investigated, Bim was the only one that was upregulated upon oprozomib exposure. P53 is well documented as a key regulator for Bcl-2 family members;[37] however, our data suggested that induction of Bim was P53-independent, implying that oprozomib acts through a different or additional mechanism independent of P53. Previous study showed that c-Jun, a transcription factor downstream of JNK, was engaged in Bim induction in glucocorticoid-induced leukemia cell death;[38] therefore, we speculated that signal transduction from JNK to Bim via c-Jun was not dependent on P53. Bim was sequestered away from Bcl-2 by interaction with dynein light chain 1 (DLC1).[39] JNK phosphorylated Bim at the DKC1 binding site, causing it to separate from DLC1. We observed enhanced Bim phosphorylation and the phosphorylated status was consistent with JNK, indicating involvement of the mitochondrial apoptotic pathway in the IRE1α branch. IRE1α possesses bifunctional kinase and RNase domain that is required for specific splicing of Xbp1 mRNA. Therefore, we also examined the contribution of RNase activity to apoptosis. The RNase activity of IRE1 removes an intron from the unspliced X-box binding protein 1(XBP1u), leading to spliced XBP1(XBP1s), the active form of the XBP1 as a transcription factor that regulates gene expression involved in ER membrane biosynthesis and chaperoning and ERAD.[40] Evidence showed that IRE1α/XBP1 is implicated in c-Myc-driven carcinogenesis and IRE1α/XBP1 signaling maintains cell viability by generating unsaturated lipids required for ER membrane homeostasis.[41] Our data showed that blockage of RNase activity slightly increased the apoptosis, supporting the cytoprotective role even at the time point when the overall tendency of UPR was pro–apoptotic. In addition to PERK and IRE1α, IPTR2-mediated disruption of Ca2+ homeostasis was also involved in oprozomib-induced apoptosis. Ca2+ is primarily stored in ER. As a dynamic intercellular messenger, Ca2+ homeostasis was strictly regulated by Ca2+-ATPase and calcium release channels. Upon apoptotic stimuli, overloading cytosolic Ca2+ triggers the initiation of apoptosis by binding to Ca2+-dependent enzymes, such as calpain and calcineurin which, in turn, activates the downstream targets, including caspase-12, representing a pathway that directly cleaved the final executor caspase-3 in a mitochondria-independent manner. Alternatively, calpain promotes apoptosis by activating Bcl-2 family members, Bax/Bid, leading to cytochrome C release. In the present study, we observed that upregulation of IPTR2, a ubiquitous intracellular Ca2+ release channel, was the leading cause of cytosolic Ca2+ accumulation. Consistent with previous studies, Ca2+ induced apoptosis relies on the calpain-caspase 12-caspase 3 cascade.

In conclusion, oprozomib evoked a complex pro–apoptotic net convergence on caspase-3 processing. Our data indicated herein a new anti–leukemia approach based on the feature that tumor cells were selectively sensitive to UPS depletion. In addition, the impact of proteasome inhibitors on CML cells was not limited with regard to the phase of the disease, indicating an alternative strategy to overcome TKI resistance that was frequently observed in advanced stages.

ACKNOWLEDGMENTS

This study was supported by the National Natural Science Foundation of Chain (No. 81600134), the Natural Science Foundation of Shaanxi Province (2019DLSF03-02), and the Clinical Research Award of the First Affiliated Hospital (XJTU1AF-CRF-2015-009).

DISCLOSURE

The authors declare no conflict of interest.

ORCID

Fang Wang https://orcid.org/0000-0003-3538-9661

REFERENCES

1. Chereda B, Melo JV. Natural course and biology of CML. *Ann Hematol*. 2015;94(Suppl. 2):S107-S121.
2. Talati C, Pinilla-Ibarz J. Resistance in chronic myeloid leukemia: definitions and novel therapeutic agents. *Curr Opin Hematol*. 2018;25:154-161.
3. Patel AB, O'Hare T, Deininger MW. Mechanisms of resistance to ABL kinase inhibition in chronic myeloid leukemia and the development of next generation ABL kinase inhibitors. *Hematol Oncol Clin North Am*. 2017;31:589-612.
4. Ao N, Chen Q, Liu G. The small molecules targeting ubiquitin-proteasome system for cancer therapy. *Comb Chem High Throughput Screen*. 2017;20:403-413.
5. Weathington NM, Mallampalli RK. Emerging therapies targeting the ubiquitin proteasome system in cancer. *J Clin Invest*. 2014;124:6-12.
6. Bazzaro M, Lee MK, Zoso A, et al. Ubiquitin-proteasome system stress sensitizes ovarian cancer to proteasome inhibitor-induced apoptosis. *Can Res*. 2006;66:3754-3763.
7. Ciechanover A. The ubiquitin-proteasome proteolytic pathway. *Cell*. 1994;79:13-21.
8. Glickman MH, Ciechanover A. The ubiquitin-proteasome proteolytic pathway: destruction for the sake of construction. *Physiol Rev*. 2002;82:373-428.
9. Gardner RG, Nelson ZW, Gottschling DE. Degradation-mediated protein quality control in the nucleus. *Cell*. 2005;120:803-815.
10. Demarchi F, Brancolini C. Altering protein turnover in tumor cells: new opportunities for anti–cancer therapies. *Drug Resist Updat*. 2005;8:359-368.
11. van den Boom J, Meyer H. VCP/p97-mediated unfolding as a principle in protein homeostasis and signaling. *Mol Cell*. 2018;69:182-194.
12. Bertolotti A, Zhang Y, Hendershot LM, Harding HP, Ron D. Dynamic interaction of BiP and ER stress transducers in the unfolded-protein response. *Nat Cell Biol*. 2000;2:326-332.
13. Sou SN, Ilieva KM, Polizzi KM. Binding of human BiP to the ER stress transducers IRE1 and PERK requires ATP. *Biochem Biophys Res Commun*. 2012;420:473-478.
14. Hetz C, Papa FR. The unfolded protein response and cell fate control. *Mol Cell*. 2018;69:169-181.
15. Merksamer PI, Papa FR. The UPR and cell fate at a glance. *J Cell Sci*. 2010;123:1003-1006.
16. Fels DR, Koumenis C. The PERK/eIF2alpha/ATF4 module of the UPR in hypoxia resistance and tumor growth. *Cancer Biol Ther*. 2006;5:723-728.
17. Mitsuda T, Omi T, Tanimukai H, et al. Sigma-1Rs are upregulated via PERK/eIF2alpha/ATF4 pathway and execute protective function in ER stress. *Biochem Biophys Res Commun*. 2011;415:519-525.
18. Mhaidat NM, Thorne R, Zhang XD, Hersey P. Involvement of endoplasmic reticulum stress in docetaxel-induced JNK-dependent apoptosis of human melanoma. *Apoptosis*. 2008;13:1505-1512.
19. Lei K, Davis RJ. JNK phosphorylation of Bim-related members of the Bcl2 family induces Bax-dependent apoptosis. *Proc Natl Acad Sci USA*. 2003;100:2432-2437.
20. Papandreou I, Denko NC, Olson M, et al. Identification of an Ire1alpha endonuclease specific inhibitor with cytotoxic activity against human multiple myeloma. *Blood*. 2011;117:1311-1314.
21. Wiel C, Lallet-Daher H, Gitenay D, et al. Endoplasmic reticulum calcium release through ITPR2 channels leads to mitochondrial calcium accumulation and senescence. *Nat Commun*. 2014;5:3792.
22. Tan Y, Dourdin N, Wu C, De Veyra T, Elce JS, Greer PA. Ubiquitous calpains promote caspase-12 and JNK activation during endoplasmic reticulum stress-induced apoptosis. *J Biol Chem*. 2006;281:16016-16024.
23. Sergeev IN. Genistein induces Ca2+ -mediated, calpain/caspase-12-dependent apoptosis in breast cancer cells. *Biochem Biophys Res Commun*. 2004;321:462-467.
24. Haferlach C, Bacher U, Schnittger S, Weiss T, Kern W, Haferlach T. Similar patterns of chromosome abnormalities in CML occur in addition to the Philadelphia chromosome with or without tyrosine kinase inhibitor treatment. *Leukemia*. 2010;24:638-640.
25. Mizrachy-Schwartz S, Cohen N, Klein S, Kravchenko-Balasha N, Levitzki A. Amino acid starvation sensitizes cancer cells to proteasome inhibition. *IUBMB Life*. 2010;62:757-763.
26. Powers GL, Rajbhandari P, Solodin NM, Bickford B, Alarid ET. The proteasome inhibitor bortezomib induces an inhibitory chromatin environment at a distal enhancer of the estrogen receptor-alpha gene. *PLoS One*. 2013;8:e81110.
27. Dufey E, Sepulveda D, Rojas-Rivera D, Hetz C. Cellular mechanisms of endoplasmic reticulum stress signaling in health and disease. 1. An overview. *Am J Physiol Cell Physiol*. 2014;307:C582-C594.
28. Obeng EA, Carlson LM, Gutman DM, Harrington WJ Jr, Lee KP, Boise LH. Proteasome inhibitors induce a terminal unfolded protein response in multiple myeloma cells. *Blood*. 2006;107:4907-4916.
29. Ri M. Endoplasmic-reticulum stress pathway-associated mechanisms of action of proteasome inhibitors in multiple myeloma. *Int J Hematol*. 2016;104:273-280.
30. Shah PP, Beverly LJ. Regulation of VCP/p97 demonstrates the critical balance between cell death and epithelial-mesenchymal transition (EMT) downstream of ER stress. *Oncotarget*. 2015;6:17725-17737.
31. Hwang J, Qi L. Quality control in the endoplasmic reticulum: crosstalk between ERAD and UPR pathways. *Trends Biochem Sci*. 2018;43:593-605.
32. Wang M, Ye R, Barron E, et al. Essential role of the unfolded protein response regulator GRP78/BiP in protection from neuronal apoptosis. *Cell Death Differ*. 2010;17:488-498.
33. Dong D, Ni M, Li J, et al. Critical role of the stress chaperone GRP78/BiP in tumor proliferation, survival, and tumor angiogenesis in transgene-induced mammary tumor development. *Can Res*. 2008;68:498-505.
34. Li J, Lee AS. Stress induction of GRP78/BiP and its role in cancer. *Curr Mol Med*. 2006;6:45-54.
35. Fu Y, Li J, Lee AS. GRP78/BiP inhibits endoplasmic reticulum BIK and protects human breast cancer cells against estrogen starvation-induced apoptosis. *Can Res*. 2007;67:3734-3740.
36. Birukova AA, Singleton PA, Gawlak G, et al. GRP78 is a novel receptor initiating a vascular barrier protective response to oxidized phospholipids. *Mol Biol Cell*. 2014;25:2006-2016.
37. Kim EM, Jung CH, Kim J, Hwang SG, Park JK, Um HD. The p53/p21 complex regulates cancer cell invasion and apoptosis by targeting Bcl-2 family proteins. *Can Res*. 2017;77:3092-3100.
38. Heidari N, Miller AV, Hicks MA, Marking CB, Harada H. Glucocorticoid-mediated BIM induction and apoptosis are regulated by Runx2 and c-Jun in leukemia cells. *Cell Death Dis*. 2012;3:e349.
39. Puthalakath H, Huang DC, O'Reilly LA, King SM, Strasser A. The proapoptotic activity of the Bcl-2 family member Bim is regulated by interaction with the dynein motor complex. *Mol Cell*. 1999;3:287-296.
40. Prischi F, Nowak PR, Carrara M, Ali MM. Phosphoregulation of Ire1 RNase splicing activity. *Nat Commun*. 2014;5:3554.

41. Zhao N, Cao J, Xu L, et al. Pharmacological targeting of MYC-regulated IRE1/XBP1 pathway suppresses MYC-driven breast cancer. *J Clin Invest*. 2018;128:1283-1299.

SUPPORTING INFORMATION

Additional supporting information may be found online in the Supporting Information section.

How to cite this article: Wang F, Wang X, Li N, et al. Prolonged unfolded protein reaction is involved in the induction of chronic myeloid leukemia cell death upon oprozomib treatment. *Cancer Sci*. 2021;112:133–143. https://doi.org/10.1111/cas.14696